

Cosmology through arc statistics I: sensitivity to Ω_m and σ_8

Michele Boldrin¹, Carlo Giocoli^{2,3,4,5}, Massimo Meneghetti^{4,6}, Lauro Moscardini^{2,3,4}, Giuseppe Tormen¹, Andrea Biviano⁷

¹ *Dipartimento di Fisica e Astronomia, Università di Padova, vicolo dell'Osservatorio 3, 35122 Padova, Italy*

² *Dipartimento di Fisica e Astronomia, Alma Mater Studiorum Università di Bologna, viale Berti Pichat 6/2, 40127 Bologna, Italy*

³ *INFN - Sezione di Bologna, viale Berti Pichat 6/2, 40127 Bologna, Italy*

⁴ *INAF - Osservatorio Astronomico di Bologna, via Ranzani 1, 40127 Bologna, Italy*

⁵ *Aix Marseille Université, CNRS, LAM (Laboratoire d'Astrophysique de Marseille), UMR 7326, 13388 Marseille, France*

⁶ *Jet Propulsion Laboratory, 4800 Oak Grove Dr., Pasadena, CA 91109, USA*

⁷ *INAF - Osservatorio Astronomico di Trieste, via G.B. Tiepolo 11, 34143 Trieste*

ABSTRACT

The next generation of large sky photometric surveys will finally be able to use arc statistics as a cosmological probe. Here we present the first of a series of papers on this topic. In particular, we study how arc counts are sensitive to the variation of two cosmological parameters: the (total) matter density parameter, Ω_m , and the normalisation of the primordial power spectrum, expressed in terms of σ_8 . Both these parameters influence the abundances of collapsed structures and their internal structure. We compute the expected number of gravitational arcs with various length-to-width ratios in mock light cones, by varying these cosmological parameters in the ranges $0.1 \leq \Omega_m \leq 0.5$ and $0.6 \leq \sigma_8 \leq 1$. We find that the arc counts dependence on Ω_m and σ_8 is similar, but not identical, to that of the halo counts. We investigate how the precision of the constraints on the cosmological parameters based on arc counts depends on the survey area. We find that the constraining power of arc statistics degrades critically only for surveys covering an area smaller than 10% of the whole sky. Finally, we consider the case in which the search for arcs is done only in frames where galaxy clusters have been previously identified. Adopting the selection function for galaxy clusters expected to be detected from photometric data in future wide surveys, we find that less than 10% of the arcs will be missed, with only a small degradation of the corresponding cosmological constraints.

Key words: Arc statistics; strong gravitational lensing; galaxy clusters; cosmology.

1 INTRODUCTION

The importance of galaxy clusters in cosmology is well known (for a review, see [Allen et al. 2011](#), and references therein). Being the most massive bound systems in the universe, they trace the latest stage of structure formation. Their abundance and mass as a function of redshift are thus highly indicative of how the growth of the cosmic density fluctuations occurs and can thus be used to constrain the matter content, the initial power spectrum normalisation and the expansion history of the universe ([Eke et al. 1998](#); [Borgani et al. 2001](#); [Reiprich & Böhringer 2002](#); [Allen et al. 2003](#); [Schuecker et al. 2003](#); [Henry 2004](#); [Vikhlinin et al. 2009](#); [Mantz et al. 2010](#); [Rozo et al. 2010](#); [Sehgal & et al. 2011](#); [Planck Collaboration et al. 2014a](#); [Benson et al. 2013](#); [Mantz et al. 2014](#)).

Moreover, galaxy clusters are essential cosmic labora-

tories where the complex interaction between baryons and dark matter can be studied in detail, in particular during merger events ([Clowe et al. 2006](#); [Merten et al. 2011](#)).

Being the most massive structures in the Universe, galaxy clusters are also the most powerful gravitational lenses ([Narayan & Bartelmann 1999](#); [Bartelmann & Schneider 2001](#); [Kneib & Natarajan 2011](#)). In particular, they are responsible for highly non-linear lensing effects taking place in their densest regions, i.e. in their cores. In this so-called “strong” lensing regime, the images of background galaxies are heavily distorted, often leading to the appearance of gravitational arcs with large length-to-width ratios (see [Kneib & Natarajan 2011](#); [Meneghetti et al. 2013](#), and references therein).

The efficiency of galaxy clusters to produce arcs with a given ratio between their length l and width w is quantified by means of their strong lensing cross section $\sigma_{l/w}$. This is

arXiv:1505.03515v2 [astro-ph.CO] 18 Jan 2016

defined as the area on the source plane where the source has to be located in order to form an arc with such a l/w ratio. To have a large strong lensing cross section, the projected mass distribution of the lens must be exceptionally dense on the plane of the sky, also called “lens plane”. Sometimes, this can be the result of projection effects (halos elongated along the line-of-sight, superposition of multiple structures at different redshifts, etc), but, generally speaking, gravitational arcs trace the highest peaks in the cosmological density field. [Bartelmann et al. \(1998\)](#) first pointed out that counting gravitational arcs may be a competitive method to constrain cosmological parameters (see e.g. [Fedeli et al. 2006](#); [Meneghetti et al. 2013](#)).

Unfortunately, strong lensing events such as gravitational arcs are rare. Given the relatively low number of arcs discovered so far and the high inhomogeneity of cluster optical surveys, the application of arc statistics in cosmology has been attempted mainly with the goal of possibly falsifying the standard cosmological model (the so-called concordance Λ CDM) rather than actually constraining cosmological parameters. For about 15 years, scientists have debated on the existence or nonexistence of a tension between the observed number of arcs and the predictions derived in the framework of the cosmological model favoured by observational data (see [Meneghetti et al. 2013](#), and references therein). Undoubtedly, arc statistics suffered so far from the lack of suitable large observational datasets for a reliable comparison to theoretical predictions. The situation is likely to change radically in the near future, thanks to the advent of large optical surveys, covering areas in the range from several thousands of square degrees ([de Jong et al. 2013](#); [The Dark Energy Survey Collaboration 2005](#)), to (almost) the full sky ([LSST Science Collaboration et al. 2009](#); [Karoji 2009](#); [Laureijs et al. 2011](#); [Spergel et al. 2013](#)).

In [Boldrin et al. \(2012\)](#) we forecasted the number of gravitational arcs visible in the future wide field survey to be performed by the ESA Euclid mission ([Laureijs et al. 2011](#)). A further step is the analysis of the sensitivity of arc statistics on cosmological parameters. In particular in this work, we focus on the dependence of arc statistics on the (total) matter density parameter Ω_m and on the normalisation of the primordial power spectrum, expressed in terms of σ_8 . More precisely, we investigate the region of the parameter space defined by $\Omega_m = [0.1 - 0.5]$, and $\sigma_8 = [0.6 - 1.0]$. We sample the parameters at intervals $\Delta\Omega_m = 0.1$ and $\Delta\sigma_8 = 0.1$, thus investigating a total of 25 different cosmological models, always making the assumption of a flat Universe ($\Omega_m + \Omega_\Lambda = 1$). To help a direct comparison with the results of [Boldrin et al. \(2012\)](#), here we assume a reference cosmology defined by the parameters ($\Omega_m = 0.272$, $\sigma_8 = 0.809$) with present Hubble parameter $H_0 = 70.4$ km/s/Mpc, in agreement with the WMAP7 results ([Komatsu et al. 2011](#)). However we will discuss also the results obtained with the assumption of the parameters recently derived by [Planck Collaboration et al. \(2014b\)](#).

The paper is organized as follows. In [Section 2](#) we briefly describe the method adopted to compute the number of arcs and to build the mock catalogs. In [Section 3](#) we present our main results, i.e. the total number of arcs and their redshift distribution as a function of Ω_m and σ_8 . [Section 4](#) is devoted to a discussion of the origin of the cosmological influence on arc statistics; we also consider how the results can change

when including the effects of possible systematics. In [Section 5](#) we discuss the agreement between the predictions obtained with our methodology and the arc counts in real surveys, using the recent results of [Xu et al. \(2015\)](#) based on the CLASH survey. Finally, in [Section 6](#) we summarise and draw our conclusions.

2 METHOD

In this section, we summarise the steps undertaken for calculating the number of arcs produced by a population of strong lenses.

2.1 Generation of lenses with MOKA

In the attempt of properly modelling all the relevant structural properties of the lenses in our calculations of $\sigma_{l/w}$, we make use of the pseudo-analytic code MOKA ([Giocoli et al. 2012a,b](#)). This code allows to generate mock cluster-size gravitational lenses in any desired cold dark matter (CDM) scenario, including features like: triaxiality and projection effects, scatter in concentration, substructures, and the presence of a brightest central galaxy, including the effects that its growth produces adiabatic contraction on the cluster dark-matter halo profile. As discussed in several earlier works based on fully numerical simulations (see e.g. [Meneghetti et al. 2003c](#); [Torri et al. 2004](#); [Meneghetti et al. 2007](#)), all these features play an important role for determining the cluster ability to produce giant arcs. The most important novelty of our work mainly lies on the adoption of very realistic simulated strong lenses, as the MOKA code allows to do.

More in detail, to generate the mock lenses we use the following prescriptions:

- the host halo mass density profile is described by the Navarro, Frenk and White (NFW) radial function ([Navarro et al. 1996](#));
- the dark matter halo concentration is derived from the mass-concentration relation proposed by [Zhao et al. \(2003\)](#), assuming log-normal scatter of $\sigma_{\ln c} = 0.25$;
- the lens halo is triaxial and the axis ratios are generated assuming the triaxial distributions derived by [Jing & Suto \(2002\)](#);
 - the spatial orientation is randomly chosen;
 - the substructure abundance follows the sub-halo mass function derived by [Giocoli et al. \(2008\)](#);
 - the substructure radial distribution follows that proposed by [Gao et al. \(2004\)](#);
 - the substructures are modelled as Single Isothermal Spheres (SISs) ([Metcalf & Madau 2001](#));
 - the mass density profile of the Brightest Cluster Galaxy (BCG) resembles the Hernquist’s profile ([Hernquist 1990](#)).

The main outcome of the MOKA code is the deflection angle map of each mock halo. From the latter, we obtain $\sigma_{l/w}$ for sources at $z_s = 2$ via ray-tracing technique. For simplicity, we consider only isolated lenses, avoiding the cases of merging haloes, even though some studies revealed the importance these events have on the amplitude of the strong lensing signal (see e.g. [Torri et al. 2004](#)). Furthermore, another source of enhancement of the signal is given by the

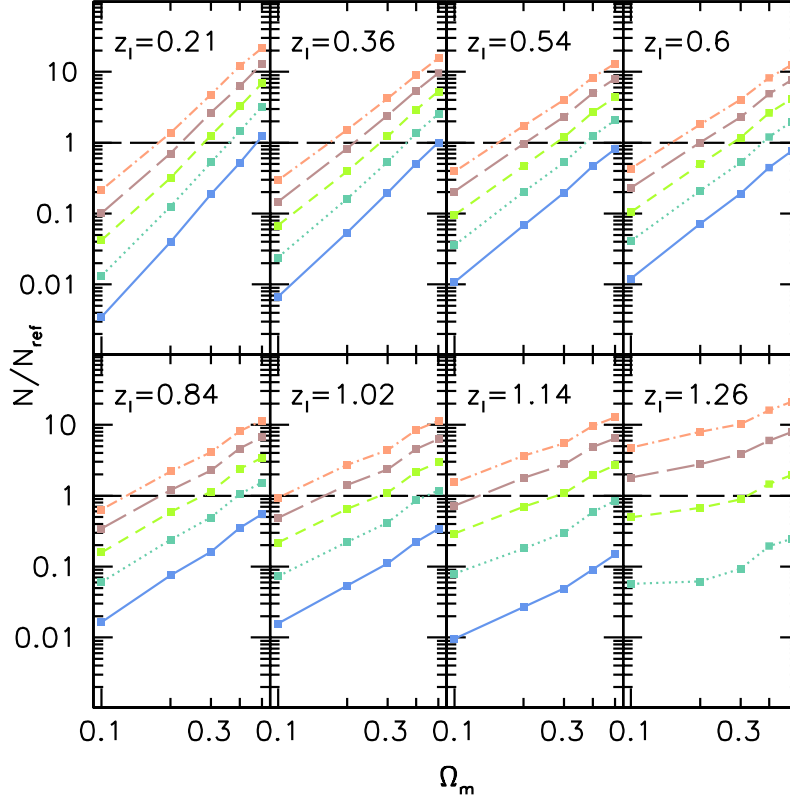


Figure 1. Number of arcs (normalised to the reference WMAP7 cosmology) as function of Ω_m and for different values of σ_8 . Different panels refer to different redshift bins between $z = 0.21$ and $z = 1.26$, as labeled. The reported counts represent the median of 128 different light-cone realisations for each combination of the cosmological parameters. Solid blue, dotted cyan, dashed green, long-dashed brown and dot-dashed dark orange lines indicate the results for $\sigma_8 = 0.6, 0.7, 0.8, 0.9$ and 1 , respectively. The results refer to arcs with $l/w \geq 10$ and sources 1σ above the mean background noise level.

large scale structure present along the line of sight, which boosts the lens projected mass on the source plane. Since beyond purpose of this paper we postpone detailed studies of those two aspects to a future work.

2.2 Number of giant arcs

We trace light-rays through a uniform grid on the lens plane towards the source plane, accounting for the position-dependent deflections. The source plane is populated with elliptical sources distributed on a regular grid. Their lensed shapes are recovered by collecting the light rays hitting them. The lengths and widths of the resulting gravitational arcs are measured using the method described in several earlier papers (see e.g. Meneghetti et al. 2003c). As in Boldrin et al. (2012), the source population has random ellipticity and an apparent size depending on the redshift (see Boldrin et al. 2012, Fig. 3.). To properly sample the region of the source plane, where sources are lensed as giant arcs, we iteratively increase the resolution of source grid near the lens caustics. Each source is then representative of an area on the source plane defined by the local resolution of the source grid. Using this area as weight, we compute $\sigma_{l/w}$, defined as the area on the source plane within which a source has to be located for being lensed as a giant arc with a given l/w (Meneghetti et al. 2008).

The number of arcs with length-to-width ratio larger than l/w , produced by a lens of mass M at redshift z_l , can be computed solving the following relation:

$$N_{l/w}(M, z_l) = \sigma_{l/w}(2) \int_{z_l}^{z_s, max} dz_s f_\sigma(z_l, z_s) n(z_s, S), \quad (1)$$

where $\sigma_{l/w}(2) \equiv \sigma_{l/w}(M, z_l, z_s = 2)$ is the strong lensing cross section for giant arcs for sources at redshift $z_s = 2$, and

$$f_\sigma \equiv \frac{\sigma_{l/w}(z_s)}{\sigma_{l/w}(z_s = 2)}$$

accounts for the scaling of $\sigma_{l/w}$ with z_s . In order to minimize the computational time, we recover the scaling function f_σ computing $\sigma_{l/w}(z_s)$ of a lens subsample, adopting different values of z_s (see for more details Boldrin et al. 2012).

A crucial ingredient is the redshift distribution of the sources exceeding a given surface brightness S , $n(z_s, S)$. We derive it by simulating an observation of the galaxies in the Hubble-Ultra-Deep-Field (HUDF) using the SkyLens code (Meneghetti et al. 2008), to a depth which is reasonable for a future wide field survey from space. As a reference, we consider the Euclid wide survey, which is expected to reach an average limiting magnitude $m_{riz} = 24.5$ (Laureijs et al. 2011). Adopting typical Euclid-like exposure times and background levels, we estimate the surface brightness limits corresponding to 1σ and 3σ above the mean background level, and use the simulated observations of the HUDF to

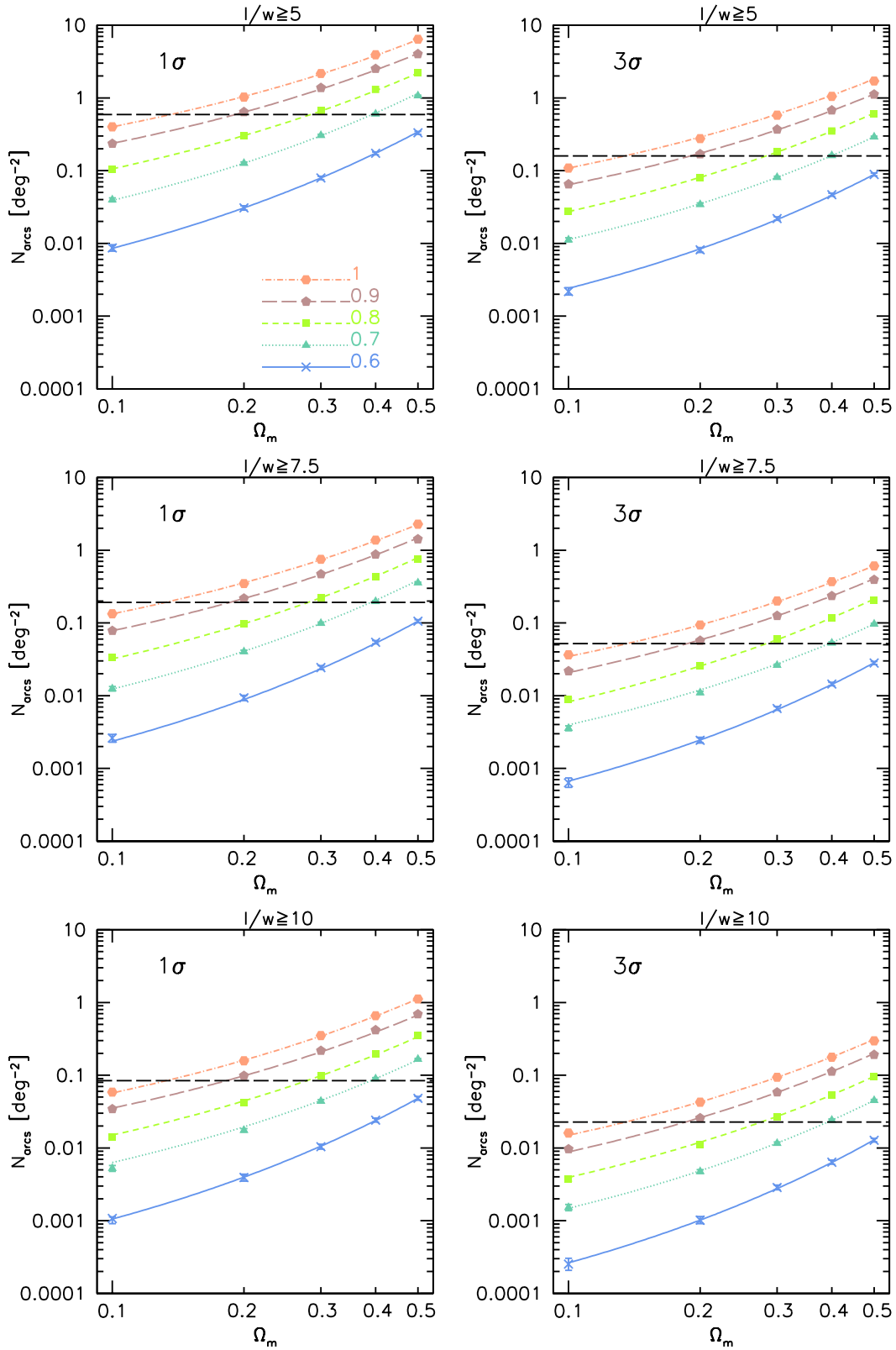


Figure 2. Number density of arcs as a function of Ω_m for different values of σ_8 . The right and left columns refer to sources detectable at 1σ and 3σ above the mean background noise level, respectively. From top to bottom, the different panels show the results for three choices of minimum l/w , namely 5, 7.5 and 10. Line and color styles are as in Fig. 1. In each panel the horizontal dashed line shows the counts in the considered reference mode..

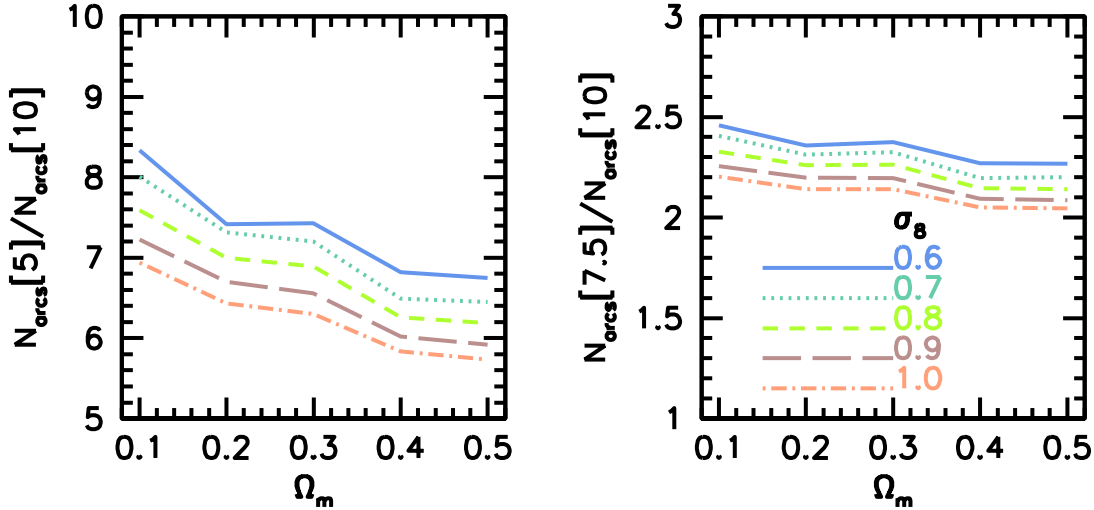


Figure 3. The abundances of arcs with $l/w \geq 5$ (left panel) and $l/w \geq 7.5$ (right panel) relative to the abundances of arcs with $l/w \geq 10$ as a function of Ω_m . Line and color styles are as in Fig. 1. The results refer to arcs detectable at 1σ above the mean background level.

measure $n(z_s, S)$. Using a subset of MOKA lenses to simulate observations of gravitational arcs, we find that we can safely neglect from the giant arc counts sources above $z_{s,max} = 6$.

For each combination of cosmological parameters, we produce a catalog of cluster-sized lenses with different masses and redshifts. We define 100 mass bins which are uniformly spaced in logarithm between 10^{13} and $10^{16} h^{-1} M_\odot$ and 8 redshift bins, having $\Delta z = 0.03$ and centered at redshifts 0.21, 0.36, 0.54, 0.6, 0.84, 1.02, 1.14, and 1.26. The choice of such redshift bins is optimised for the expected redshift distribution of the lenses producing giant arcs, which we derived in Boldrin et al. (2012) for a Euclid-like survey. For each combination of redshift and mass we use MOKA to generate 100 halos with different structural properties and measure their $\sigma_{l/w}$, from which we can derive the number of giant arcs they produce, as discussed above.

The catalog of lenses is then used to generate 128 realisations of lens distributions (light-cones). In each light-cone, which subtends an area of 15,000 square degrees, we calculate the number of lenses of mass M and redshift z_l according to the Sheth & Tormen (1999) mass function, and estimate the total number of arcs by summing up the contributions from each individual lens. Finally, we combine the different light-cones to measure the median number of arcs per square degree and the relative scatter as a function of the considered cosmological parameters.

3 RESULTS

3.1 Number of arcs as a function of redshift

We begin by discussing how the arc counts change as a function of cosmology in different redshift bins. In Fig. 1 we show the number of arcs, normalized to the reference WMAP7 cosmology, as function of Ω_m . The different panels refer to the eight redshifts where the calculations were performed. Different colors and line styles are used to display the re-

sults for several values of σ_8 : solid blue, dotted cyan, dashed green, long-dashed brown and dot-dashed dark orange lines refer to $\sigma_8=0.6, 0.7, 0.8, 0.9$ and 1 , respectively. Long-dashed black horizontal lines correspond to unity, i.e. to the reference cosmology. The lack of a blue solid line in the last panel is due to the inefficiency of clusters at $z_l = 1.26$ to produce giant arcs in the cosmology with $\sigma_8 = 0.6$. As expected, at all redshifts, the arc counts grow as a function of Ω_m and as a function of σ_8 , indicating that the abundance of giant gravitational arcs is higher in cosmological models with more matter and higher normalisation of the power spectrum of the primordial density fluctuations.

We also notice that the change of arc counts as a function of cosmology depends on the lens redshift. The dependence on Ω_m is stronger at lower redshift, and flattens off as z_l increases. On the contrary, it appears that the value of σ_8 affects the results more significantly at high redshift.

While the results in Fig. 1 refer to arcs with $l/w \geq 10$ and sources above the 1σ background level, the trends remain similar for other l/w ratios and detection limits.

3.2 The total number of arcs

From the distributions obtained from the 128 different light-cone realizations, we measure the median number of arcs per square degree expected in each cosmological model. This has been done by performing a spline interpolation through the above-mentioned 8 redshifts up to a maximum lens redshift of $z_l = 1.5$.

In the reference WMAP7 cosmology, the expected number densities of arcs per square degree with $l/w \geq 5, 7.5$, and 10 are $0.594 \pm 0.016, 0.194 \pm 0.006$, and 0.085 ± 0.003 , respectively. These are in excellent agreement with our estimates reported in Boldrin et al. (2012), although these were obtained using a larger number of redshift bins and avoiding the interpolation.

In Fig. 2, we show the median arc number counts per

square degree as a function of Ω_m . We also show how the counts vary by changing the value of σ_8 , using the same color and line styles used in Fig. 1. From top to bottom, we show the results for $l/w \geq 5$, 7.5, and 10, respectively. The left and the right panels refer to detections at 1- and 3σ above the level of the background. Obviously, the results show the same dependence on Ω_m and σ_8 reported in Fig. 1.

We also see that the ratios between counts of arcs with different l/w depend on the cosmological parameters. As shown in Fig. 3, for low Ω_m , the abundance of arcs with $l/w \geq 5$ or $l/w \geq 7.5$, relative to that of arcs with $l/w \geq 10$, is higher, indicating that halos in these cosmological models have smaller critical lines and are thus less efficient at producing large distortions. The ratios also depend on σ_8 ; in cosmologies with higher σ_8 halos are able to produce a higher abundance of arcs with large l/w . The results (here shown only for sources 1σ above the mean background level) are insensitive to the assumed detection limit. Therefore, in the following discussion we will show the results only for arcs detectable at the 1σ level. We will also focus on arcs with $l/w \geq 10$.

The upper panel in Fig. 4 shows the difference in the arc counts relative to the reference WMAP7 cosmology in the $\Omega_m - \sigma_8$ plane. Within the ranges explored in this work, we may find differences of up to one order of magnitude for the predicted arc counts between cosmological models. We also notice that the cosmological parameters Ω_m and σ_8 are degenerate with respect to the arc counts. Indeed, the same number of arcs is expected in cosmologies whose combination of Ω_m and σ_8 lays in a banana-like region extending from the upper left to the bottom right corner of the plane. The origin of this degeneracy will be better discussed in Section 4.1. Interestingly, a Planck-like cosmology with $\Omega_m = 0.3086$ and $\sigma_8 = 0.8288$ (Planck Collaboration et al. 2014b) produces 54% more arcs than the reference WMAP7 cosmology.

We find that in the case of the reference WMAP7 model, the equation describing the degeneracy curve between the cosmological parameters has the following form:

$$\Omega_m = A\sigma_8^2 + B\sigma_8 + C, \quad (2)$$

where $A = 1.771$, $B = -3.952$ and $C = 2.31$. Such function is given by the white line in the upper panel of Fig. 4.

In the attempt to quantify the uncertainty in the arc counts, we define the 1σ uncertainty on the number counts as $\sigma \equiv (\sigma_{CV}^2 + \sigma_P^2)^{1/2}$, where σ_{CV} is the cosmic variance, which is estimated from the 16th and 84th percentiles of the distributions derived from the 128 light-cone realisations of each tested cosmological model. The other term appearing in the equation, $\sigma_P \equiv \sqrt{N}$, is the associated Poisson noise on the number counts.

In the bottom panel of Fig. 4, we perform an error analysis showing the levels corresponding to 1, 3, and 5σ deviations (from dark to light colors) from the WMAP7 and the Planck cosmologies in the $\Omega_m - \sigma_8$ plane. The results were obtained assuming a survey covering 15,000 sq. degrees of the sky to the depth expected for the Euclid mission. It is interesting to notice that a survey with the Euclid characteristics will be able to distinguish these two cosmological models at more than 5σ level.

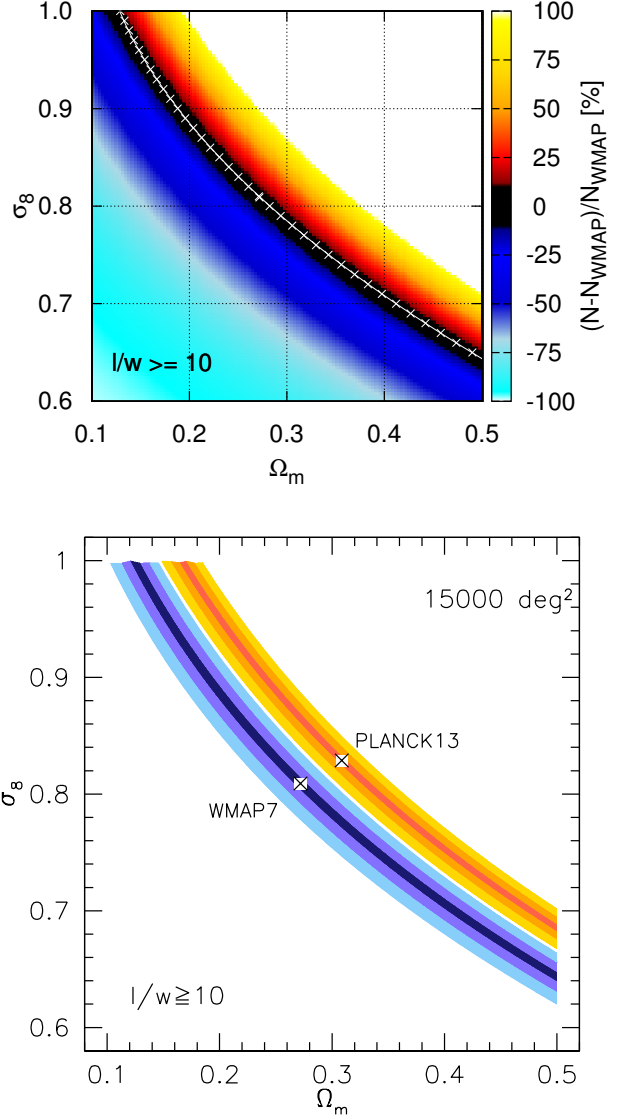


Figure 4. *Upper panel:* difference in the arc counts with respect to the reference WMAP7 cosmology in the $\Omega_m - \sigma_8$ plane. The results are shown for arcs with $l/w \geq 10$ detectable at 1σ above the background level. The white crosses represent the cosmological models having the same arc counts as the reference WMAP7 model [relation (2)]. *Bottom panel:* levels corresponding to 1, 3, and 5σ deviations (from dark to light colors) from the WMAP7 (blue) and the Planck (yellow) cosmologies in the $\Omega_m - \sigma_8$ plane, assuming a 15,000 deg^2 survey to the expected depth of the Euclid wide survey. The crosses indicate the position of the two reference models.

4 DISCUSSION

4.1 Influence of the cosmological parameters on arc statistics

In this section we will discuss in more detail some aspects of the influence of Ω_m and σ_8 on arc statistics. In general, the cosmological parameters play an important role in arc statistics through the lens mass function and their strong lensing cross section, the latter depending on the geometry

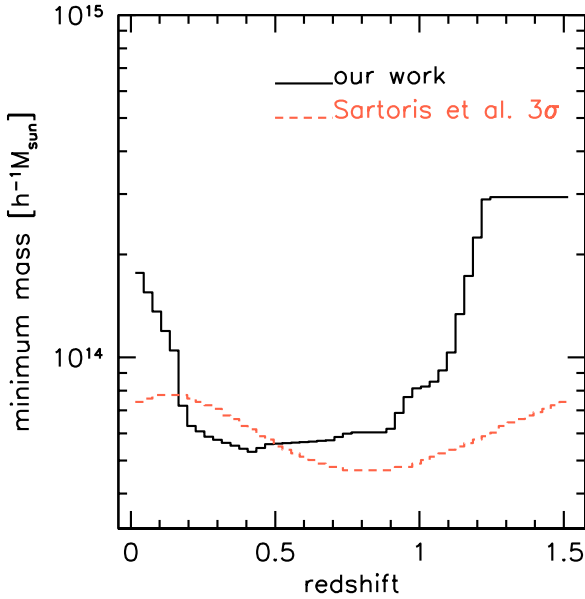


Figure 5. The strong lensing selection function (black solid curve), i.e. the minimum galaxy cluster mass expected to produce critical lines for sources located at $z_s = 2$ (Meneghetti et al. 2010a; Boldrin et al. 2012). For comparison, the red dashed curve represents the minimum mass of galaxy clusters which are expected to be detected above three times the rms of the field galaxy counts in the Euclid photometric survey (?).

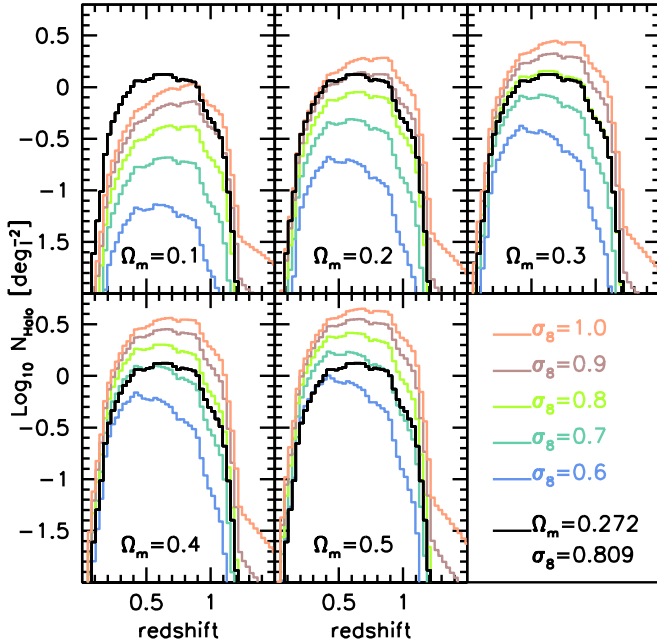


Figure 6. Number density of expected strong lenses as a function of redshift, for cosmologies with different Ω_m and σ_8 . Plots from left to right and from up to bottom refer to increasing values of Ω_m . Different colors represent counts for various values of σ_8 , as labeled on the bottom right. The black line shown in all panels represents the results for the reference WMAP7 model.

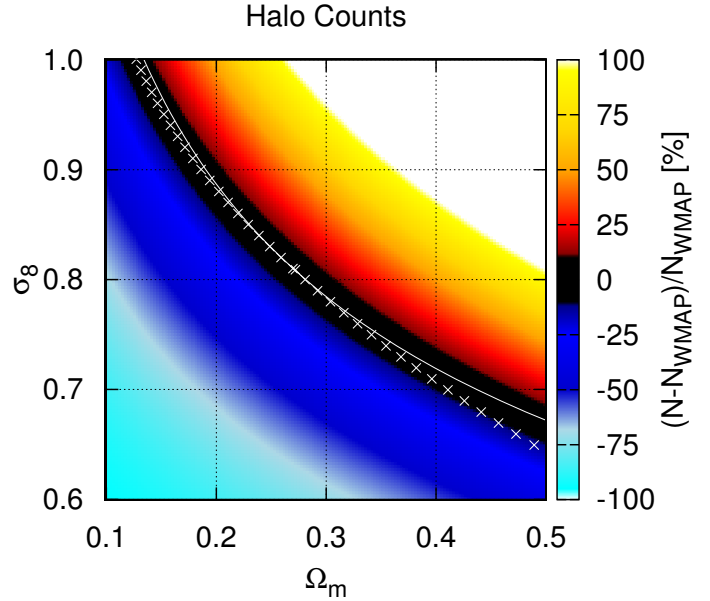


Figure 7. Relative difference of halo counts on the σ_8 - Ω_m plane with respect to the reference WMAP7 model. The white crosses represent the degeneracy curve relative to the arc counts, while the white solid line refers to the degeneracy curve for halo counts.

of the Universe and on the structural properties of the lens halo.

In particular, the number of arcs is directly related to the number of lenses able to produce arcs. Following Meneghetti et al. (2010a, 2011), this can be estimated including in the mass function describing the lens distribution a sharp cut at the minimum mass corresponding to the smallest systems in which we expect to find critical lines for sources at $z_s = 2$. The shape of the adopted selection function as a function of redshift is shown by the black curve in Fig. 5 (see also Boldrin et al. 2012).

In Fig. 6, we present the number density (given per square degree) of the lenses as a function of redshift. In each panel, we keep fixed Ω_m as labeled and we vary the value for σ_8 , using the color code indicated on the bottom right. To facilitate the comparison, the lens number density in the reference WMAP7 cosmology is shown in black in all panels. From the figure, the strong effect of the different matter density on the lens abundances and the anticipated structure formation originated by a higher power spectrum normalization are clear.

In Fig. 7, adopting the same color code as in the upper panel of Fig. 4, we show the difference in the lens counts relative to the reference WMAP7 cosmology in the $\Omega_m - \sigma_8$ plane. The white solid curve in the figure represents the degeneracy between Ω_m and σ_8 for the halo counts, for which we find the following relation:

$$\sigma_8 (\Omega_m / 0.272)^{0.304} = 0.809. \quad (3)$$

Even if with some differences, this curve is close to the relation (shown by the white crosses) representing the degeneracy we found in the $\Omega_m - \sigma_8$ plane for the arc counts (see also Fig. 4): this is clearly due to the fact that the most important ingredient for arc statistics is the lens mass func-

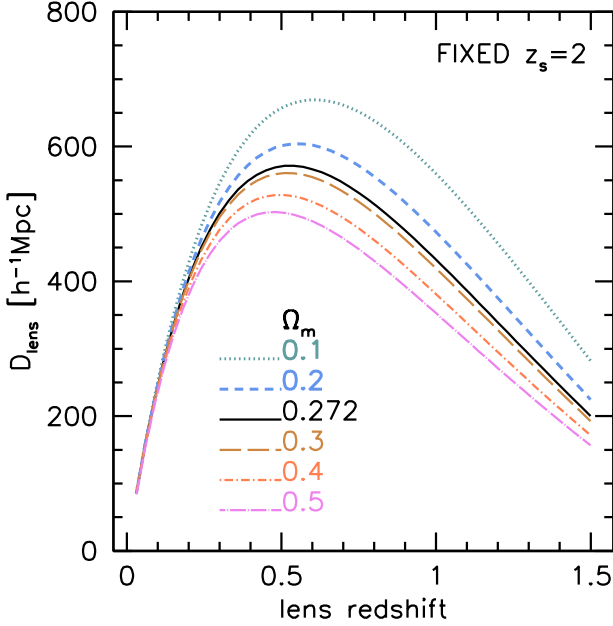


Figure 8. Lensing distance for different values of Ω_m . Sources are kept fixed at redshift $z_s = 2$.

tion. However, if one compares the amplitude of the count variation by looking at the width of the coloured strips, it is evident that the arc density is more sensitive to the cosmological parameters than the simple halo density: consequently, a wide survey of gravitational arcs could potentially give significant constraints.

The larger sensitivity of arc statistics is due to the cosmological dependence of the other main ingredients, such as the angular diameter distances of lenses and sources and the lens structural properties. We know that the first condition for an axially symmetric lens to act like a strong lens is that in some points \vec{x} on the lens plane the condition

$$\kappa(\vec{x}) > 1 \quad (4)$$

occurs, where $\kappa \equiv \Sigma(\vec{x})/\Sigma_{cr}$ is the so-called convergence, $\Sigma(\vec{x})$ is the lens projected mass density and

$$\Sigma_{cr} \equiv \frac{c^2}{4\pi G} D_{lens}^{-1} \quad (5)$$

represents the critical value of the two-dimensional mass density in order to have strong lensing effects. The quantity D_{lens} is the so-called *lensing distance*, defined as

$$D_{lens} \equiv \frac{D_{LS} D_L}{D_S}, \quad (6)$$

where D_S , D_L and D_{LS} are the angular diameter distances of the source, of the lens and between source and lens, respectively. Although for elliptical lenses we have to add the effect of shear to the condition (4), we can infer, to first approximation, what are the system configurations which are more efficient in producing strong lensing features by investigating how D_{lens} changes in the different cosmological models, once the lens properties and the source redshifts are kept fixed. We remind the reader that D_{lens} contains the full dependence on the geometry of the system and does not depend on σ_8 , but only on Ω_m . We fix the source position

at redshift $z_s = 2$ and we study $D_{lens}(z_l)$, that is we keep fixed the length of the lensing system and we move the lens from the observer towards the source plane. The results are shown in Fig. 8: we see that increasing the value of Ω_m , the strong lensing efficiency reaches its maximum at lower lens redshifts. In particular the peak around which the production of gravitational arcs is expected to be boosted shifts from $z \approx 0.6$ to $z \approx 0.4$ when the value of Ω_m is increased from 0.1 to 0.5.

The effect of the anticipation of structure formation due to a higher value of σ_8 (Giocoli et al. 2007, 2012b) has consequences on several halo structural properties that may influence the size of $\sigma_{l/w}$. Considering the concentration parameter, at fixed σ_8 , large Ω_m values lead to larger concentrations because the structures form and grow in denser environments. At the same time, keeping fixed the value of Ω_m , in cosmologies with high σ_8 the concentration increases because of both the higher contrast between primordial perturbations and background, and the anticipated formation time (Neto et al. 2007; Giocoli et al. 2012b; Macciò et al. 2008).

Halo triaxiality is also an important feature that depends on cosmological parameters (Despali et al. 2014; Bonamigo et al. 2015). In particular, the level of sphericity of a halo, which is directly related to the ratio between its minor and major semi-axes a/c , is an increasing function of σ_8 and a decreasing function of Ω_m . As an example, if we consider haloes with a mass equal to $7.5 \times 10^{14} h^{-1} M_\odot$ at redshift $z = 0.54$ in a cosmological model with $\Omega_m = 0.3$, the median ratio among 128 realizations varies from $a/c = 0.353^{+0.049}_{-0.056}$ in a model with $\sigma_8 = 0.6$, to $a/c = 0.417^{+0.057}_{-0.066}$ in a model with $\sigma_8 = 1.0$. The quoted uncertainties correspond to 1σ errors. On the other hand, if we fix $\sigma_8 = 0.8$, the ratio changes from $a/c = 0.419^{+0.058}_{-0.066}$ in a model with $\Omega_m = 0.1$, to $a/c = 0.388^{+0.053}_{-0.061}$ in a model with $\Omega_m = 0.5$.

4.2 Effects of completeness and cluster selection function

In the following subsections we will discuss how our results change when we take into account the lack of completeness and when we introduce a realistic photometric galaxy cluster selection function.

4.2.1 The effect of sample completeness and survey area

Let us consider here the case in which a fraction of arcs are missed, independently of the properties of the lens configurations (l/w , z_l , z_s). This may happen because some arcs may escape detection for some particular configurations of the light distribution within the cluster, or when the separation between cluster and foreground galaxies is made difficult by the lack of precise color information. The total arc counts may also diminish because we are performing our search in a reduced effective area, smaller than the one of the running survey. In this situation losing 10% of the counts is equivalent to observe a portion of sky 10% smaller than the original survey. The obvious consequence of a reduction of the number of observed arcs is that the Poissonian uncertainty grows and can start to dominate with respect to the

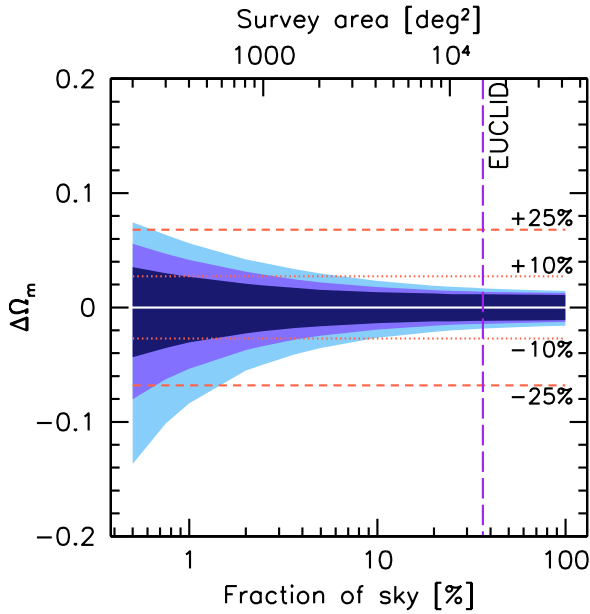


Figure 9. The amplitude of the 3σ error bar on Ω_m as a function of the survey area. The vertical dashed line shows the size of the future Euclid wide survey. The red horizontal dotted and dashed lines represent a variation of Ω_m corresponding to $\pm 10\%$ and $\pm 25\%$, respectively.

cosmic variance, when accounting for the total error budget. To quantify this effect, in Fig. 9 we show, as a function of the fraction of the sky covered by the arc search, the variation of the 3σ error bar on the parameter Ω_m , when the value of σ_8 is a priori fixed to its reference value ($\sigma_8 = 0.809$), as it may happen if independently measured from other cosmological probes. Dark, medium and light blue regions refer to the cases of arcs with $l/w \geq 5$, 7.5 and 10, respectively, while the horizontal dotted (dashed) lines indicate an accuracy of 10 (25) per cent on Ω_m . From the figure it is clear that arcs with $l/w \geq 5$, being more numerous, give stronger constraints and are less affected by possible incompleteness problems. However, there is a difficulty when dealing with them because they can look like simple edge-on galaxies. For this reason the loss and misidentification of arcs are expected to depend on l/w , being stronger for low- l/w ratios. From this point of view, Fig. 9 is quite encouraging: if the survey area is sufficiently wide (larger than 10% of the whole sky), or equivalently if the arc finders are sufficiently efficient, the error budget is dominated by cosmic variance and there is not a significant difference in the constraining power between using arcs with $l/w \geq 5$ or with $l/w \geq 10$. We remind that the SDSS (York et al. 2000) has an area of about 10,000 deg², while the Euclid wide survey is expected to cover 15,000 deg² (Laureijs et al. 2011).

4.2.2 The effect of the cluster selection function

Due to the high computational cost of the algorithms for arc detection, a possible strategy in future wide surveys is to run these codes only on small-size frames where galaxy clusters have been previously identified. Obviously, this originates a reduction of the effective number of arcs, which is strongly

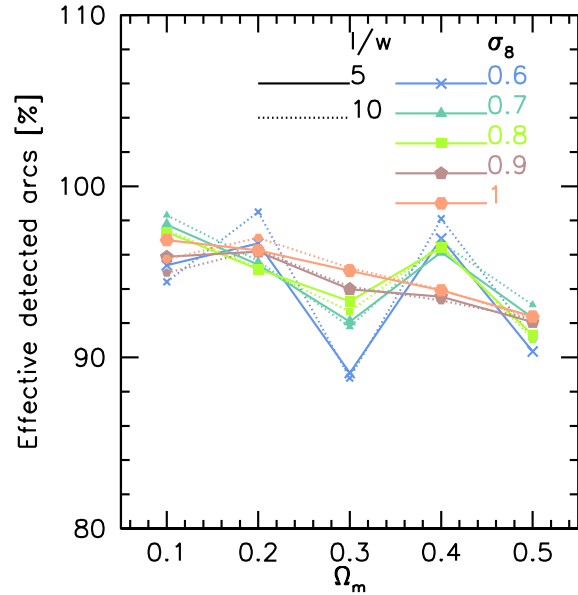


Figure 10. Percentage of arcs effectively detected by considering only lenses having a mass larger than the Euclid cluster photometric selection function. Different color refer to different values of σ_8 , as labeled; solid and dotted lines are for arcs with $l/w \geq 5$ and 10.

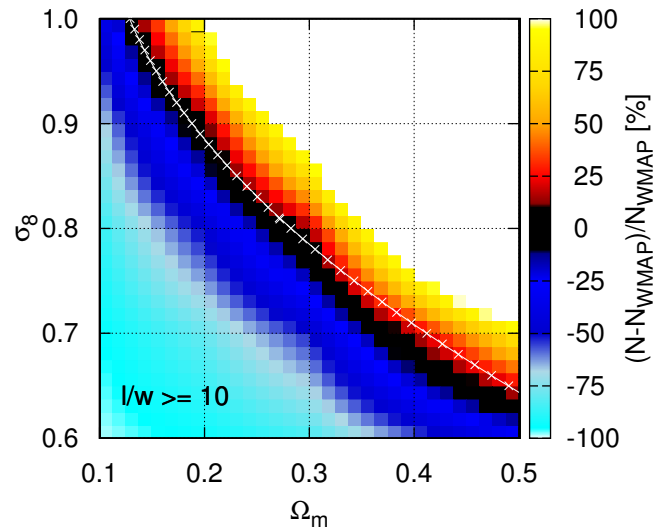


Figure 11. As the upper plot of Fig. 4, but for arcs produced by lenses having a mass larger than the Euclid cluster photometric selection function (?). The crossed line represents the degeneracy curve obtained when no selection function is applied.

dependent on the specific cluster selection function of the survey.

As a worked example, here we consider again the future ESA Euclid mission. Given the amount and quality of its data covering an area of 15,000 deg², there will be at least three main ways to identify galaxy clusters: (i) from photometric data, (ii) from spectroscopic data, and (iii) from cosmic shear maps. As shown in ?, the one based on photo-

metric data (see, for example, Bellagamba et al. 2011, and references therein) is expected to be largely the most efficient one. In this case, the minimum mass of galaxy clusters having a number of members larger than 3 times the r.m.s. of the field galaxy counts is expected to be between $5 \times 10^{13} M_{\odot}/h$ and $8 \times 10^{13} M_{\odot}/h$ in the redshift range here considered (?). Compared to the minimum mass needed to produce critical lines for sources located at redshift $z_s = 2$ (see Fig. 5), the Euclid cluster selection is then slightly higher on a limited redshift range only, namely between $z = 0.2$ and $z = 0.5$. This means that limiting the search for arcs to frames where galaxy clusters have been already identified is expected to not reduce dramatically the number of detected arcs. This is confirmed in Fig. 10, where we show the fraction of arcs that can be effectively detected following this strategy. Same colors indicate same values of σ_8 , as labeled in the figure, while solid and dotted lines refer to arcs with $l/w \geq 5$ and 10, respectively. For the cosmological models here considered, the reduction varies between 2 and 10 per cent and is almost independent of l/w . For the reference WMAP7 model, the percentage of effectively detected arcs remains about 95 per cent.

In Fig. 11 we show the relative differences in the arc counts between each cosmological model and the reference WMAP7 cosmology, considering only arcs produced by galaxy clusters above the Euclid photometric selection function. In the figure, the color scale is identical to that adopted in the upper panel of Fig. 4. The white crosses represent the degeneration curve we found considering the total number of arcs, i.e. without applying the cluster selection function. Although similar, the curve changes in a non negligible way, especially considering extreme values of the parameters. This underlines the importance of taking into account every kind of selection function when combining theory and observations in arc statistic studies, avoiding possible systematics.

The presence of strong lensing features like arcs can represent a complementary way to confirm the presence of a galaxy cluster. Moreover arcs can be used to improve the estimates of the mass of galaxy clusters, a fundamental ingredient to fully exploit the evolution of their abundance as cosmological probe. For this reason it is important to compute what is the fraction of the galaxy clusters identified in the Euclid photometric survey, which are able to produce at least one giant arc. The result for the reference WMAP7 cosmology as a function of redshift is shown in Fig. 12 for arcs with $l/w \geq 5$, 7.5 and 10 (black solid, red dashed and green long-dashed lines, respectively). Typical mean values are around 1 per cent, 0.33 per cent and 0.15 per cent for $l/w \geq 5$, 7.5 and 10, respectively. From the figure we notice that the strong lens fraction peaks around $z = 0.5$: this behaviour is a combined effect between the well of the photometric selection function around redshift $z = 0.75$ and the peak – around the same redshifts – of the strong lens counts. Interestingly, for redshift $z \geq 1.3$ the percentage tends to vanish. Finally we notice that the fact that the strong lensing selection function can be smaller than the photometric cluster one would allow in principle to add extra objects to the Euclid cluster sample by looking for strong lensing features only. However this would require to run the algorithms for arc detection blindly in different areas of the survey. Considering the reference WMAP7 model and arcs

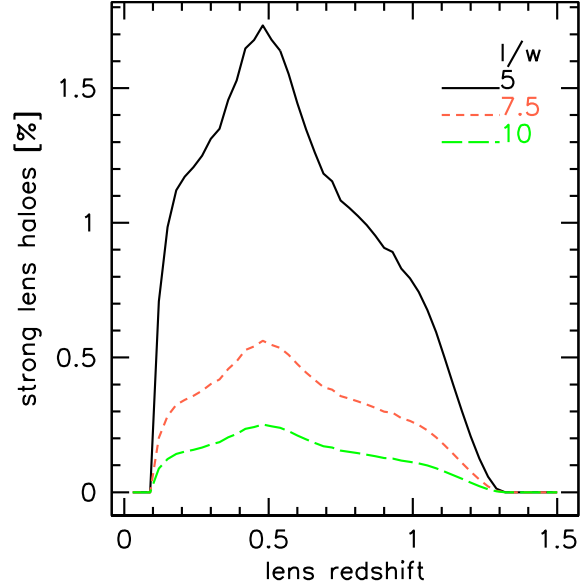


Figure 12. Fraction of galaxy clusters having a mass larger than the Euclid cluster photometric selection function producing at least one giant arc. Results are shown for the reference WMAP7 model. Different line styles refer to different length-to-width ratios, as labeled.

with $l/w \geq 5$, the gain would correspond to approximately 300 extra objects only, all having a relatively low redshift ($0.2 \leq z \leq 0.5$).

Therefore, we can conclude that arc statistics represents a complementary tool to identify galaxy clusters or eventually to prove their presence. In particular, arcs with a small l/w ratio are the best tracers, since they are more numerous, but, at the same time, they are the more difficult to identify because of their similarity with non-lensed galaxies. Finally, our results underline that the codes for arc identification can be run on single frames where galaxy clusters have been already detected with no consequences on the cosmological predictive power of arc statistics.

5 A TEST-BED FOR THE METHOD: THE CLASH SURVEY

While this paper focuses on the sensitivity of arc statistics to cosmological parameters like Ω_m and σ_8 , it is worth mentioning that another paper has been recently submitted by our collaborators Xu et al. (2015) to compare theoretical predictions of arc abundances in a Λ CDM cosmological model and observations. More precisely, in this other work MOKA has been used to build up halos reproducing the properties of the X-ray selected galaxy clusters belonging to the CLASH sample (Postman et al. 2012). Numerical hydro-dynamical simulations tailored to reproduce the CLASH selection function (Meneghetti et al. 2014) are also used to derive theoretical predictions. Thus, the work of Xu et al. (2015) provides the best opportunity for validating our methodology against more complex models of the cluster mass distribution and against observed clusters with a known selection function.

The results of this study show that there is an excellent

agreement between expectations based on MOKA halos and numerical simulations and the arc counts in the CLASH clusters. More specifically, the lensing efficiency measured in the CLASH sample is 4 ± 1 arcs (with $l > 6''$ and $l/w > 7$) per cluster. MOKA simulations return exactly the same number (4 ± 1), while numerical simulations give 3 ± 1 arcs per cluster. Therefore, according to Xu et al. (2015), in terms of efficiency to produce long and thin arcs, observations and simulations based on MOKA and numerical hydrodynamical techniques come into full agreement. It is particularly significant that the methodology we have developed for modeling cluster lenses for arc-statistics calculations is fully capturing the complexity of numerically simulated halos, as evinced from the fact that the cross sections for giant arcs of MOKA generated halos are well matching those of the halos described in Meneghetti et al. (2014).

6 CONCLUSIONS

In this work we have investigated how the number of gravitational arcs depends on cosmology, focusing our attention on the (total) matter density parameter Ω_m and on the initial normalisation power spectrum parameter σ_8 . In more detail we have considered the ranges $\Omega_m = [0.1 - 0.5]$ and $\sigma_8 = [0.6 - 1.0]$. Our main results can be summarised as follows.

- We confirm that arc statistics is very sensitive to the couple of parameters $\Omega_m - \sigma_8$. In particular we find that the expected number of arcs is an increasing function of both parameters: this is mostly due to the fact that increasing these parameters boosts the number of lenses.
- The efficiency in producing arcs in cosmologies with high values of σ_8 is larger, since it has an effect also on the structure formation time, that in turn affects some lens structural properties (mainly concentration and triaxiality) relevant for strong lensing.
- A strong degeneracy exists between the two considered cosmological parameters for the number of arcs N_{arcs} ; for the reference WMAP7 model this is expressed by the relation (2), that is similar, but not equal, in shape to the degeneracy derived from galaxy cluster counts (see eq. 3). The differences between the two arise from the non negligible contribution to $\sigma_{l/w}$ given by the lens structural properties – triaxiality, asymmetries, concentration, substructures and the BCG – and the lensing distance relation.
- Arcs with small l/w ratio are more suitable to constrain cosmological parameters, since they are more numerous. On the other hand, they could be more difficultly identified in the surveys because of their similarity with non-lensed galaxies. We find that if the survey area is sufficiently larger (more than 10% of the full sky) the error budget is dominated by cosmic variance, and the constraining power of arc counts becomes almost independent of the value of l/w . In particular a survey covering $15,000 \text{ deg}^2$ will be able to distinguish at more than 5σ level the two cosmological models supported by WMAP7 and Planck CMB data.
- Considering future wide surveys, like the ESA Euclid mission, we find that searching for arcs only in frames where galaxy clusters have been previously detected will produce a loss of 2-10% of arcs only (depending on the cosmological

model) and a consequent limited degradation of the constraining power of arc counts. This suggests that it will be not necessary to run the computationally expensive algorithms for arc detection on whole wide surveys.

In this paper we have discussed the potentiality and the capability of the giant arc statistic to constrain the matter density and the initial power spectrum normalisation parameter in light of the large data-sets that will become available from future wide-field surveys.

ACKNOWLEDGEMENTS

We thank Barbara Sartoris, Cosimo Fedeli and Peter Schneider for useful discussions on the Euclid cluster selection function. CG's research is part of the project GLENCO, funded under the European Seventh Framework Programme, Ideas, Grant Agreement n. 259349. CG thanks CNES for financial support. LM acknowledge financial contributions from contracts ASI/INAF/I/023/12/0, by the PRIN MIUR 2010-2011 “The dark Universe and the cosmic evolution of baryons: from current surveys to Euclid” and by the PRIN INAF 2012. We are grateful to the referee Prasenjit Saha for his useful comments.

REFERENCES

- Allen S. W., Evrard A. E., Mantz A. B., 2011, *ARA&A*, 49, 409
- Allen S. W., Schmidt R. W., Fabian A. C., Ebeling H., 2003, *MNRAS*, 342, 287
- Bartelmann M., Huss A., Colberg J. M., Jenkins A., Pearce F. R., 1998, *A&A*, 330, 1
- Bartelmann M., Schneider P., 2001, *Physics Report*, 340, 291
- Bellagamba F., Maturi M., Hamana T., Meneghetti M., Miyazaki S., Moscardini L., 2011, *MNRAS*, 413, 1145
- Benson B. A., de Haan T., Dudley J. P., Reichardt C. L., Aird K. A., Andersson K., Armstrong R., Ashby M. L. N., Bautz M., Bayliss M., Bazin G., Bleem L. E., Brodwin M., Carlstrom J. E., Chang C. L., Cho H. M., Clocchiatti e. a., 2013, *ApJ*, 763, 147
- Boldrin M., Giocoli C., Meneghetti M., Moscardini L., 2012, *MNRAS*, 427, 3134
- Bonamigo M., Despali G., Limousin M., Angulo R., Giocoli C., Soucail G., 2015, *MNRAS*, 449, 3171
- Borgani S., Rosati P., Tozzi P., Stanford S. A., Eisenhardt P. R., Lidman C., Holden B., Della Ceca R., Norman C., Squires G., 2001, *ApJ*, 561, 13
- Clowe D., Bradač M., Gonzalez A. H., Markevitch M., Randall S. W., Jones C., Zaritsky D., 2006, *ApJ*, 648, L109
- de Jong J. T. A., Verdoes Kleijn G. A., Kuijken K. H., Valentijn E. A., 2013, *Experimental Astronomy*, 35, 25
- Despali G., Giocoli C., Tormen G., 2014, *MNRAS*, 443, 3208
- Eke V. R., Cole S., Frenk C. S., Patrick Henry J., 1998, *MNRAS*, 298, 1145
- Fedeli C., Meneghetti M., Bartelmann M., Dolag K., Moscardini L., 2006, *A&A*, 447, 419
- Gao L., White S. D. M., Jenkins A., Stoehr F., Springel V., 2004, *MNRAS*, 355, 819

- Giocoli C., Meneghetti M., Bartelmann M., Moscardini L., Boldrin M., 2012a, MNRAS, 421, 3343
- Giocoli C., Meneghetti M., Ettori S., Moscardini L., 2012b, MNRAS, 426, 1558
- Giocoli C., Moreno J., Sheth R. K., Tormen G., 2007, MNRAS, 376, 977
- Giocoli C., Tormen G., van den Bosch F. C., 2008, MNRAS, 386, 2135
- Henry J. P., 2004, ApJ, 609, 603
- Hernquist L., 1990, ApJ, 356, 359
- Jing Y. P., Suto Y., 2002, ApJ, 574, 538
- Karoji H., 2009, in IAC Talks, Astronomy and Astrophysics Seminars from the Instituto de Astrofísica de Canarias Hyper Suprime-Cam (HSC) project for the SUBARU telescope. p. 146
- Kneib J.-P., Natarajan P., 2011, A&A Rev., 19, 47
- Komatsu E., Smith K. M., Dunkley J., Bennett C. L., Gold B., Hinshaw G., Jarosik N., Larson D., et al. 2011, ApJS, 192, 18
- Laureijs R., Amiaux J., Arduini S., Auguères J., Brinchmann J., Cole R., Cropper M., Dabin C., Duvet L., et al. 2011, ArXiv e-prints 1110.3193
- LSST Science Collaboration Abell P. A., Allison J., Anderson S. F., Andrew J. R., Angel J. R. P., Armus L., Arnett D., Asztalos S. J., Axelrod T. S., et al. 2009, ArXiv e-prints 0912.0201
- Macciò A. V., Dutton A. A., van den Bosch F. C., 2008, MNRAS, 391, 1940
- Mantz A., Allen S. W., Rapetti D., Ebeling H., 2010, MNRAS, 406, 1759
- Mantz A. B., Allen S. W., Morris R. G., Rapetti D. A., Applegate D. E., Kelly P. L., von der Linden A., Schmidt R. W., 2014, MNRAS, 440, 2077
- Meneghetti M., Argazzi R., Pace F., Moscardini L., Dolag K., Bartelmann M., Li G., Oguri M., 2007, A&A, 461, 25
- Meneghetti M., Bartelmann M., Dahle H., Limousin M., 2013, Space Sci.Rev.
- Meneghetti M., Bartelmann M., Moscardini L., 2003c, MNRAS, 346, 67
- Meneghetti M., Fedeli C., Pace F., Gottlöber S., Yepes G., 2010a, A&A, 519, A90+
- Meneghetti M., Fedeli C., Zitrin A., Bartelmann M., Broadhurst T., Gottlöber S., Moscardini L., Yepes G., 2011, A&A, 530, A17+
- Meneghetti M., Melchior P., Grazian A., De Lucia G., Dolag K., Bartelmann M., Heymans C., Moscardini L., Radovich M., 2008, A&A, 482, 403
- Meneghetti M., Rasia E., Vega J., Merten J., Postman M., Yepes G., Sembolini F., Donahue M., et al. 2014, ApJ, 797, 34
- Merten J., Coe D., Dupke R., Massey R., Zitrin A., Cypriano E. S., Okabe N., Frye B., Braglia F. G., Jiménez-Teja Y., Benítez N., Broadhurst T., Rhodes J., Meneghetti M. et al., 2011, MNRAS, 417, 333
- Metcalf R. B., Madau P., 2001, MNRAS, 563, 9
- Narayan R., Bartelmann M., 1999, in Dekel A., Ostriker J. P., eds, Formation of Structure in the Universe Gravitational lensing. p. 360
- Navarro J. F., Frenk C. S., White S. D. M., 1996, ApJ, 462, 563
- Neto A. F., Gao L., Bett P., Cole S., Navarro J. F., Frenk C. S., White S. D. M., Springel V., Jenkins A., 2007, MNRAS, 381, 1450
- Planck Collaboration Ade P. A. R., Aghanim N., Armitage-Caplan C., Arnaud M., Ashdown M., Atrio-Barandela F., Aumont J., Baccigalupi C., Banday A. J., et al. 2014b, A&A, 571, A16
- Planck Collaboration Ade P. A. R., Aghanim N., Armitage-Caplan C., Arnaud M., Ashdown M., Atrio-Barandela F., Aumont J., Baccigalupi C., Banday A. J., et al. 2014a, A&A, 571, A20
- Postman M., Coe D., Benítez N., Bradley L., Broadhurst T., Donahue M., Ford H., Graur O., Graves G., Jouvel S., et al. 2012, ApJS, 199, 25
- Reiprich T. H., Böhringer H., 2002, ApJ, 567, 716
- Rozo E., Wechsler R. H., Rykoff E. S., Annis J. T., Becker M. R., Evrard A. E., Frieman J. A., Hansen S. M., Hao J., Johnston D. E., Koester B. P., McKay T. A., Sheldon E. S., Weinberg D. H., 2010, ApJ, 708, 645
- Schuecker P., Böhringer H., Collins C. A., Guzzo L., 2003, A&A, 398, 867
- Sehgal N., et al. 2011, ApJ, 732, 44
- Sheth R. K., Tormen G., 1999, MNRAS, 308, 119
- Spergel D., Gehrels N., Breckinridge J., Donahue M., Dressler A., Gaudi B. S., Greene T., Guyon O., et al. 2013, ArXiv e-prints 1305.5422
- The Dark Energy Survey Collaboration 2005, ArXiv Astrophysics e-prints arXiv:astro-ph/0510346
- Torri E., Meneghetti M., Bartelmann M., Moscardini L., Rasia E., Tormen G., 2004, MNRAS, 349, 476
- Vikhlinin A., Kravtsov A. V., Burenin R. A., Ebeling H., Forman W. R., Hornstrup A., Jones C., Murray S. S., Nagai D., Quintana H., Voevodkin A., 2009, ApJ, 692, 1060
- Xu B., Postman M., Meneghetti M., Seitz S., Zitrin A., Merten J., Maoz D., Frye B., Umetsu K., Zheng W., Bradley L., Vega J., Koekemoer A., 2015, ArXiv e-prints 1511.04002
- York D. G., Adelman J., Anderson Jr. J. E., Anderson S. F., SDSS Collaboration 2000, AJ, 120, 1579
- Zhao D. H., Jing Y. P., Mo H. J., Börner G., 2003, ApJ, 597, L9